

A novel theoretical approach for the study of resonances in weakly bound systems

Mahamadun Hasan¹, Shamim Haque Mondal¹, Murshid Alam¹,
Tasrief Surungan² and Md Abdul Khan^{1*}

¹Department of Physics, Aliah University, IIA/27, Newtown, Kolkata-700160, India

²Department of Physics, Hasanuddin University, Makassar-90245, Indonesia

E-mail: *drakhan.rsm.phys@gmail.com; drakhan.phys@aliah.ac.in (*Corresponding author)

Abstract. In this paper, a novel theoretical scheme is presented to investigate resonant levels in weakly bound nuclear systems by the use of isospectral potentials. In this scheme, a new potential is constructed which is strictly isospectral with the original shallow-well potential and has properties that are desirable to calculate resonances more accurately and easier. Effectiveness of the method has been demonstrated in terms of its application to the first 0^+ resonances in the neutron-rich isotopes ${}^A\text{C}$ ($\equiv {}^{A-2}\text{C}+n+n$) in the three-body cluster model for $A=18, 20$.

17 PACS number(s): 21.45.+v, 21.10.Dr, 27.10.+h

Keywords: Halo nuclei, resonance, isospectral potential.

1. Introduction

The discovery of halo nuclei (neutron-halo and proton-halo) in the neighborhood of drip lines is one of the major achievements of the advancements of the radioactive ion-beam facilities. Halo structure is characterized by a relatively stable and denser core surrounded by weakly bound one or more valence nucleon(s) giving rise to long extended tail in the density distribution. This low-density tail is supposed to be the consequence of quantum mechanical tunneling of the last nucleon(s) through a-shallow barrier following an attractive well that appears due to the short-range nuclear interaction, at energies smaller than the height of the barrier. In halo nuclei, one seldom finds any excited bound states because of the utmost support one bound state at energies less than 1 MeV. Halo nuclei have high scientific significance as they exhibit one or more resonance state(s) just above the binding threshold. The observed halo nuclei- ${}^{17}\text{B}$, ${}^{19}\text{C}$ show one-neutron halo; ${}^6\text{He}$, ${}^{11}\text{Li}$, ${}^{11,14}\text{Be}$ show two-neutron halo; ${}^8\text{B}$, ${}^{26}\text{P}$ show one proton-halo; ${}^{17}\text{Ne}$, ${}^{27}\text{S}$ show two proton-halo and ${}^{14}\text{Be}$, ${}^{19}\text{B}$ show four neutron-halo structure respectively [1, 2, 3, 4, 5, 6]. Halo-nuclei is characterized by their unusually large r.m.s. matter radii (larger than the liquid-drop model prediction of $R_A \propto A^{1/3}$) [7, 8] and sufficiently small two-nucleon separation energies (typically less than 1 MeV). Tanaka et al. 2010. [6] observed of a large reaction cross-section in the drip-line nucleus ${}^{22}\text{C}$, Kobayashi et al. 2012 [2], conducted research on one- and two-neutron removal reactions from the most neutron-rich carbon isotopes, Gaodefroy et al 2012 [9] carried a direct mass measurements of ${}^{19}\text{B}$, ${}^{22}\text{C}$, ${}^{29}\text{F}$, ${}^{31}\text{Ne}$, ${}^{34}\text{Na}$ and some other light exotic nuclei. Togano et al, 2016 [10] studied interaction cross-section of the

two-neutron halo nucleus ^{22}C .

Nuclear matter distribution profile of such nuclei has an extended low-density tail forming a halo around the more localized dense nuclear core. Thus, in addition to bound state properties, continuum spectra is another significant parameter that is highly involved in the investigation of structure and interparticle interactions in the exotic few-body systems like the halo nuclei. It is worth stating here that the study of resonances is of particular interest in many branches of physics involving weakly bound systems in which only few bound states are possible.

In the literature survey, we found three main theoretical approaches that were used to explore the structure of 2n-halo nuclei. The first one is the microscopic model approach in which the valence neutrons are supposed to move around the conglomerate of other nucleons (protons and neutrons) without having any stable core. The second one is the three-body cluster model in which the valence nucleons are assumed to move around the structureless inert core. And the third one is the microscopic cluster model in which the valence nucleons move around the deformed excited core [11, 12, 13]. There are several theoretical approaches which are employed for computation of resonant states. Some of those are the positive energy solution of the Faddeev equation [14], complex coordinate rotation (CCR) [15, 16], the analytic computation of bound state energies [17], the algebraic version of resonating group method (RGM) [18], continuum-discretized coupled-channels (CDCC) method clubbed to the cluster-orbital shell model (COSM) [19], hyperspherical harmonics method (HHM) for scattering states [20], etc. In most of the theoretical approaches, Jacobi coordinates are used to derive the relative coordinates separating the center of mass motion.

One of the most challenging obstacles that are involved in the calculation of resonances in any weakly bound nucleus is the large degree of computational error. In our case, we overcome this obstacle by adopting a novel theoretical approach by interfacing the algebra of supersymmetric quantum mechanics with the algebra involved in the hyperspherical harmonics expansion method. In this scheme, one can handle the ground state as well as the resonant states on the same footing. The technique is based on the fact that, for any arbitrarily given potential (say, U), one can construct a family of isospectral potentials (\hat{U}), in which the latter depends on an adjustable parameter (λ). And when the original potential has a significantly low and excessively wide barrier (poorly supporting the resonant state), λ can be chosen judiciously to enhance the depth of the well together with the height of the barrier in \hat{U} . This enhanced well-barrier combination in \hat{U} facilitates trapping of the particle which in turn facilitates the computation of resonant state more accurately at the same energy, as that in the case of U . This is because, U and \hat{U} are **strictly isospectral**.

To test the effectiveness of the scheme we apply the scheme to the first 0^+ resonant states of the carbon isotopes ^AC , for A equal to 18 and 20 respectively. We chose three-body ($2n+^{A-2}\text{C}$) cluster model for each of the above isotopes, where outer core neutrons move around the relatively heavier core ^{A-2}C . The lowest eigen potential derived for the three-body systems has a shallow well following a skinny and sufficiently wide barrier. This skinny-wide barrier gives rise to a large resonance width. One can, in principle, find quasi-bound states in such a shallow potential, but that poses a difficult numerical task. For a finite height of the barrier, a particle can temporarily be trapped in the shallow well when its energy is close to the resonance energy. However, there is a finite possibility that the particle may creep in and tunnel out through the barrier. Thus, a more accurate calculation of resonance energy is easily masked by the large resonance width resulting from a large tunneling probability due to a low barrier height. Hence, a straightforward calculation of the resonance energies of such systems fails to yield accurate results.

We adopt the hyperspherical harmonics expansion method (HHEM) [21] to solve the three-body Schrödinger equation in relative coordinates. In HHEM, three-body relative wavefunction is expanded in a complete set of hyperspherical harmonics. The substitution of the wavefunction

in the Schrödinger equation and use of orthonormality of HH gives rise to an infinite set of coupled differential equations (CDE). The method is an essentially exact one, involving no other approximation except an eventual truncation of the expansion basis subject to the desired precision in the energy and the capacity of available computer. However, hyperspherical convergence theorem [22] permits extrapolation of the data computed for the finite size of the expansion basis, to estimate those for even larger expansion bases. However, the convergence of HH expansion being significantly slow one needs to solve a large number of CDE's to achieve desired precision causing another limitation, hence we used the hyperspherical adiabatic approximation (HAA) [23] to construct single differential equation (SDE) to be solved for the lowest eigen potential, $U_0(\rho)$ to get the ground state energy E_0 and the corresponding wavefunction $\psi_0(\rho)$ [24].

We next derive the isospectral potential $\hat{U}(\lambda, \rho)$ following algebra of the SSQM [25, 26, 27]. Finally, we solve the SDE for $\hat{U}(\lambda, \rho)$ for various positive energies to get the wavefunction. We then compute the probability density corresponding to the wavefunction for finding the particle within the deep-sharp well following the enhanced barrier. A plot of probability density as a function of energy shows a sharp peak at the resonance energy. The actual width of resonance can be obtained by back-transforming the wave function $\hat{\psi}(\lambda, \rho)$ corresponding to $\hat{U}(\lambda, \rho)$ to $\psi(\rho)$ of $U(\rho)$.

The paper is organized as follows. In sections 2, we briefly review the HHE method. In section 3, we present a precise description of the SSQM algebra to construct the one-parameter family of isospectral potential $\hat{U}(\lambda, \rho)$. The results of our calculation are presented in section 4 while conclusions are drawn in section 5.

2. Hyperspherical Harmonics Expansion Method

For a the three-body model of the nuclei $A-2\text{C}+n+n$, the relatively heavy core $A-2\text{C}$ is labeled as particle 1, and two valence neutrons are labelled as particle 2 and 3 respectively. Thus there are three possible partitions for the choice of Jacobi coordinates. In any chosen partition, say the i^{th} partition, particle labelled i plays the role of spectator while remaining two particles form the interacting pair. In this partition the Jacobi coordinates are defined as

$$\vec{x}_i = a_i(\vec{r}_j - \vec{r}_k); \vec{y}_i = \frac{1}{a_i} \left(\vec{r}_i - \frac{m_j \vec{r}_j + m_k \vec{r}_k}{m_j + m_k} \right); \vec{R} = \frac{\sum_{i=1}^3 m_i \vec{r}_i}{M} \quad (1)$$

where i, j, k form a cyclic permutation of 1,2,3. The parameter $a_i = \left[\frac{m_j m_k M}{m_i (m_j + m_k)^2} \right]^{\frac{1}{4}}$; m_i, \vec{r}_i are the mass and position of the i^{th} particle and $M (= \sum_{i=1}^3 m_i)$, \vec{R} are those of the centre of mass (CM) of the system. Then in terms of Jacobi coordinates, the relative motion of the three-body system can be described by the equation

$$\left\{ -\frac{\hbar^2}{2\mu} \nabla_{x_i}^2 - \frac{\hbar^2}{2\mu} \nabla_{y_i}^2 + V_{jk}(\vec{x}_i) + V_{ki}(\vec{x}_i, \vec{y}_i) + V_{ij}(\vec{x}_i, \vec{y}_i) - E \right\} \Psi(\vec{x}_i, \vec{y}_i) = 0 \quad (2)$$

where $\mu = \left[\frac{m_i m_j m_k}{M} \right]^{\frac{1}{2}} \rightarrow$ is the reduced mass of the system, V_{ij} represents the interaction potential between the particles i and j , $x_i = \rho \cos \phi_i$; $y_i = \rho \sin \phi_i$; $\phi_i = \tan^{-1} \left(\frac{y_i}{x_i} \right)$; $\rho = \sqrt{x_i^2 + y_i^2}$. The hyperradius ρ together with five angular variables $\Omega_i \rightarrow \{\phi_i, \theta_{x_i}, \phi_{x_i}, \theta_{y_i}, \phi_{y_i}\}$ constitute hyperspherical coordinates of the system. The Schrödinger equation in hyperspherical variables (ρ, Ω_i) becomes

$$\left\{ -\frac{\hbar^2}{2\mu} \frac{1}{\rho^5} \frac{\partial^2}{\partial \rho^2} - \frac{\hbar^2}{2\mu} \frac{4}{\rho} \frac{\partial}{\partial \rho} + \frac{\hbar^2}{2\mu} \frac{\hat{K}^2(\Omega_i)}{\rho^2} + V(\rho, \Omega_i) - E \right\} \Psi(\rho, \Omega_i) = 0. \quad (3)$$

In Eq.(3) $V(\rho, \Omega_i) = V_{jk} + V_{ki} + V_{ij}$ is the total interaction potential in the i^{th} partition and $\hat{\mathcal{K}}^2(\Omega_i)$ is the square of the hyperangular momentum operator satisfying the eigenvalue equation

$$\hat{\mathcal{K}}^2(\Omega_i)\mathcal{Y}_{K\alpha_i}(\Omega_i) = K(K+4)\mathcal{Y}_{K\alpha_i}(\Omega_i) \quad (4)$$

K is the hyperangular momentum quantum number and $\alpha_i \equiv \{l_{x_i}, l_{y_i}, L, M\}$, $\mathcal{Y}_{K\alpha_i}(\Omega_i)$ are the hyperspherical harmonics (HH) for which a closed analytic expressions can be found in ref. [14]. In the HHEM, $\Psi(\rho, \Omega_i)$ is expanded in the complete set of HH corresponding to the partition "i" as

$$\Psi(\rho, \Omega_i) = \sum_{K\alpha_i} \frac{\psi_{K\alpha_i}(\rho)}{\rho^{5/2}} \mathcal{Y}_{K\alpha_i}(\Omega_i) \quad (5)$$

Use of Eq. (5), in Eq. (3) and application of the orthonormality of HH leads to a set of coupled differential equations (CDE) in ρ

$$\left\{ -\frac{\hbar^2}{2\mu} \frac{d^2}{d\rho^2} + \frac{\hbar^2}{2\mu} \frac{(K+3/2)(K+5/2)}{\rho^2} - E \right\} \psi_{K\alpha_i}(\rho) + \sum_{K'\alpha'_i} \mathcal{M}_{K\alpha_i}^{K'\alpha'_i} \psi_{K'\alpha'_i}(\rho) = 0. \quad (6)$$

where

$$\mathcal{M}_{K\alpha_i}^{K'\alpha'_i} = \int \mathcal{Y}_{K\alpha_i}^*(\Omega_i) V(\rho, \Omega_i) \mathcal{Y}_{K'\alpha'_i}(\Omega_i) d\Omega_i. \quad (7)$$

The infinite set of CDE's represented by Eq. (6) is truncated to a finite set by retaining all K values up to a maximum of K_{max} in the expansion (5). For a given K , all allowed values of α_i are included. The size of the basis states is further restricted by symmetry requirements and associated conserved quantum numbers. The reduced set of CDE's are then solved by adopting hyperspherical adiabatic approximation (HAA) [23]. In HAA, the CDE's are approximated by a single differential equation assuming that the hyperradial motion is much slower compared to hyperangular motion. For this reason, the angular part is first solved for a fixed value of ρ . This involves diagonalization of the potential matrix (including the hyper centrifugal repulsion term) for each ρ -mesh point and choosing the lowest eigenvalue $U_0(\rho)$ as the lowest eigen potential [24]. Then the energy of the system is obtained by solving the hyperradial motion for the chosen lowest eigen potential ($U_0(\rho)$), which is the effective potential for the hyperradial motion

$$\left\{ -\frac{\hbar^2}{2\mu} \frac{d^2}{d\rho^2} + U_0(\rho) - E \right\} \psi_0(\rho) = 0 \quad (8)$$

Renormalized Numerov algorithm subject to appropriate boundary conditions in the limit $\rho \rightarrow 0$ and $\rho \rightarrow \infty$ is then applied to solve Eq. (8) for $E (\leq E_0)$. The hyper-partial wave $\psi_{K\alpha_i}(\rho)$ is given by

$$\psi_{K\alpha_i}(\rho) = \psi_0(\rho) \chi_{K\alpha_i,0}(\rho) \quad (9)$$

where $\chi_{K\alpha_i,0}(\rho)$ is the $(K\alpha_i)^{th}$ element of the eigenvector, corresponding to the lowest eigen potential $U_0(\rho)$.

3. Construction of Isospectral Potential

In this section we present a bird's eye view of the scheme of construction of one parameter family of isospectral potentials. We have from Eq. (8)

$$U_0(\rho) = E_0 + \frac{\hbar^2}{2\mu} \frac{\psi_0''(\rho)}{\psi_0(\rho)} \quad (10)$$

In 1-D supersymmetric quantum mechanics, one defines a superpotential for a system in terms of its ground state wave function (ψ_0) [25] as

$$W(\rho) = -\frac{\hbar}{\sqrt{2m}} \frac{\psi_0'(\rho)}{\psi_0(\rho)}. \quad (11)$$

The energy scale is next shifted by the ground state energy (E_0) of the potential $U_0(\rho)$, so that in this shifted energy scale the new potential become

$$U_1(\rho) = U_0(\rho) - E_0 = \frac{\hbar^2}{2\mu} \frac{\psi_0''(\rho)}{\psi_0(\rho)} \quad (12)$$

having its ground state at zero energy. One can then easily verify that $U_1(\rho)$ is expressible in terms of the superpotential via the Riccati equation

$$U_1(\rho) = W^2(\rho) - \frac{\hbar}{\sqrt{2m}} W'(\rho). \quad (13)$$

By introducing the operator pairs

$$\left. \begin{aligned} A^\dagger &= -\frac{\hbar}{\sqrt{2m}} \frac{d}{d\rho} + W(\rho) \\ A &= \frac{\hbar}{\sqrt{2m}} \frac{d}{d\rho} + W(\rho) \end{aligned} \right\} \quad (14)$$

the Hamiltonian for U_1 becomes

$$H_1 = -\frac{\hbar^2}{2m} \frac{d^2}{d\rho^2} + U_1(\rho) = A^\dagger A. \quad (15)$$

The pair of operators A^\dagger, A serve the purpose of creation and annihilation of nodes in the wave function. Next we introduce a partner Hamiltonian H_2 , corresponding to the SUSY partner potential U_2 of U_1 as

$$H_2 = -\frac{\hbar^2}{2m} \frac{d^2}{d\rho^2} + U_2(\rho) = AA^\dagger \quad (16)$$

where

$$U_2(\rho) = W^2(\rho) + \frac{\hbar}{\sqrt{2m}} W'(\rho). \quad (17)$$

Energy eigen values and wavefunctions corresponding to the SUSY partner Hamiltonians H_1 and H_2 are connected via the relations

$$\left. \begin{aligned} E_n^{(2)} &= E_{n+1}^{(1)}, E_0^{(1)} = 0 \quad (n = 0, 1, 2, 3, \dots), \\ \psi_n^{(n)} &= \sqrt{E_{n+1}^{(1)}} A \psi_{n+1}^{(1)} \\ \psi_{n+1}^{(1)} &= \sqrt{E_n^{(2)}} A^\dagger \psi_n^{(2)} \end{aligned} \right\} \quad (18)$$

where $E_n^{(i)}$ represents the energy of the n^{th} excited state of H_i ($i=1, 2$). Thus H_1 and H_2 have identical spectra, except the fact that the partner state of H_2 corresponding to the ground state of H_1 is absent in the spectrum of H_2 [25]. Hence the potentials U_1 and U_2 are **not strictly isospectral**.

However, one can construct, a one parameter family of **strictly isospectral** potentials $\hat{U}_1(\lambda, \rho)$, exploiting the fact that for a given $U_1(\rho)$, $U_0(\rho)$ and $W(\rho)$ are not unique (see Eqs. (12) &

(13)), since the Riccati equation is a nonlinear one. Following [25, 26, 28], it can be shown that the most general superpotential satisfying Riccati equation for $U_1(\rho)$ (Eq. (16)) is given by

$$\hat{W}(\rho) = W(\rho) + \frac{\hbar}{\sqrt{2m}} \frac{d}{d\rho} \log[I_0(\rho) + \lambda] \quad (19)$$

where λ is a constant of integration, and I_0 is given by

$$I_0(\rho) = \int_{\rho'=0}^{\rho} [\psi_0(\rho')]^2 d\rho', \quad (20)$$

in which $\psi_0(\rho)$ is the normalized ground state wave function of $U_0(\rho)$. The potential

$$\hat{U}_1(\lambda, \rho) = \hat{W}^2(\rho) - \frac{\hbar}{\sqrt{2m}} \hat{W}'(\rho) = U_1(\rho) - 2 \frac{\hbar^2}{2m} \frac{d^2}{d\rho^2} \log[I_0(\rho) + \lambda], \quad (21)$$

has the same SUSY partner $U_2(\rho)$. $\hat{U}_1(\lambda, \rho)$ has its ground state at zero energy with the corresponding wavefunction given by

$$\hat{\psi}_1(\lambda, \rho) = \frac{\psi_1}{I_0 + \lambda}. \quad (22)$$

Hence, potentials $\hat{U}_1(\lambda, \rho)$ and $U_1(\rho)$ are **strictly isospectral**. The parameter λ is arbitrary in the intervals $-\infty < \lambda < -1$ and $0 < \lambda < \infty$. $I_0(\rho)$ lies between 0 and 1, so the interval $-1 \leq \lambda \leq 0$ is forbidden, in order to bypass singularities in $\hat{U}_1(\lambda, \rho)$. For $\lambda \rightarrow \pm\infty$, $\hat{U}_1 \rightarrow U_1$ and for $\lambda \rightarrow 0+$, \hat{U}_1 develops a narrow and deep attractive well in the vicinity of the origin. This well-barrier combination effectively traps the particle giving rise to a sharp resonance. This method has been tested successfully for 3D finite square well potential [29] choosing parameters capable of supporting one or more resonance state(s) in addition to one bound state. Nuclei $^{18,20}\text{C}$ have in their ground states $T = 1, J^\pi = 0^+$ and there exists a resonance state of the same J^π . Thus, the forgoing procedure starting from the ground state of $^{18,20}\text{C}$ will give $T = 1, J^\pi = 0^+$ resonance(s). In an attempt to search for the correct resonance energy, we compute the probability of finding the system within the well region of the potential $\hat{U}_1(\lambda, \rho)$ corresponding to the energy $E (> 0)$ by integrating the probability density up to the top of the barrier:

$$G(E) = \int_{\rho'=0}^{\rho_B} |\hat{\psi}_E(\rho', \lambda)|^2 d\rho' \quad (23)$$

where ρ_B indicates position of the top of the barrier component of the potential $\hat{U}_1(\lambda, \rho)$ for a chosen λ . Here $\hat{\psi}_E(\lambda, \rho)$ that represents the solution of the potential $\hat{U}_1(\lambda, \rho)$, corresponding to a positive energy E , is normalized to have a constant amplitude in the asymptotic region. Plot of the quantity $G(E)$ against increasing E ($E > 0$) shows a peak at the resonance energy $E = E_R$. Choice of λ has to be made judiciously to avoid numerical errors entering in the wavefunction in the extremely narrow well for $\lambda \rightarrow 0+$. The width of resonance can be obtained from the mean life of the state using the energy-time uncertainty relation. The mean life is reciprocal to the decay constant. And the decay constant is the product of the number of hit per unit time on the barrier and the corresponding probability of tunneling through the barrier.

4. Results and discussions

Eq.(6) is solved for the GPT n-n potential [31] and core-n SBB potential [32]. The range parameter for the core-n potential b_{cn} is slightly adjusted to match the experimental ground state spectra. The calculated two-neutron separation energies (S_{2n}), the relative convergence

in energy ($= \frac{E(K_{max}+4) - E(K_{max})}{E(K_{max}+4)}$) and the rms matter radii (R_A) for gradually increasing K_{max} are listed in Table 1 for both of ^{18}C and ^{20}C . Although the computed results indicate a clear convergence trend with increasing K_{max} , it is far away from full convergence even at $K_{max} = 24$. For this reason, we used an extrapolation technique successfully used for atomic systems [32, 33] as well as for nuclear system [34], to get the converged value of about 4.91 MeV for ^{18}C and 3.51 MeV for ^{20}C as shown in columns 2 and 4 of Table 2. Partial contribution of the different partial waves to the two-neutron separation energies corresponding to $l_x = 0, 1, 2, 3, 4$ are presented in Table 3. Variation of the two-neutron separation as a function of K_{max} is shown in Figure 1 for both the nuclei ^{18}C and ^{20}C . In Figure 2 we have shown the relative convergence trend in energies as a function of K_{max} . In Figures 3 and 4 we have presented a 3D view of the correlation density profile of the halo nuclei ^{18}C and ^{20}C . While in Figures 5 and 6 we have shown the 2D projection of the 3D probability density distribution. The figures clearly indicate the halo structure of the nuclei comprising a dense core surrounded by low density tail.

After getting the ground state energy and wavefunctions we constructed the isospectral potential invoking principles of SSQM to investigate the resonant states. The lowest eigen potential obtained for the ground states of ^{18}C and ^{20}C as shown in yellow lines in Figures 7 and 8 exhibits shallow well followed by a broad and low barrier. This low well-barrier combination may indicate resonant states. However, since the well is very shallow and the barrier is not sufficiently high, the resonance width is very large and a numerical calculation of the resonant state is quite challenging. Hence, we constructed the one-parameter family of isospectral potentials $\hat{U}(\lambda, \rho)$ following Eq.(19) by appropriate selection λ parameter values, such that a narrow and sufficiently deep well followed by a high barrier is obtained which are also shown in Figures 7 and 8 in representative cases. The enhanced well-barrier combination effectively traps the particles to form a strong resonant state. Calculated parameters of the isospectral potential for some λ values, along with the original lowest eigen potential $U_0(\rho)$ (which corresponds to $\lambda \rightarrow \infty$) are presented in Table 4. One can, for example, note from Table 4 under ^{18}C that, when λ changes from $= 0.1$ to 0.0001 , the depth of the well increases from -24.2 MeV at 2.7 fm to -247.6 MeV at 1.3 fm while the height of the barrier increases from 5.4 MeV at 5.1 fm to 121.5 MeV at 1.9 fm. The same trend is observed for ^{20}C also. Thus the application of SSQM produces a **dramatic effect** in the isospectral potential $\hat{U}_1(\lambda, \rho)$ as λ approaches $0+$. Further smaller positive values of λ are not desirable since that will make the well too narrow to compute the wave functions accurately by a standard numerical technique. The probability of trapping, $G(E)$, of the particle within the enhanced well-barrier combination as a function of the particle energies E shown in Figures 9 and 10 exhibit resonance peak at the energies $E_R \simeq 1.89$ MeV for ^{18}C and at energy $E_R \simeq 3.735$ MeV for ^{20}C respectively. It is interesting to see that the resonance energy is independent of the λ parameter. The enhancement of accuracy in the determination of E_R is the principal advantage of using Supersymmetric formalism. Since $\hat{U}_1(\lambda; \rho)$ is strictly isospectral with $U(\rho)$, any value of λ is admissible in principle. However, a judicious choice of λ is necessary for accurate determination of the resonance energy. The calculated two-neutron separation energies are in excellent agreement with the observed values 4.910 ± 0.030 MeV for ^{18}C and 3.510 ± 0.240 MeV for ^{20}C [35] and also with results of Yamaguchi et al [36] as presented in Table 5. The calculated RMS matter radii also agree fairly with the experimental values [37].

5. Summary and conclusions

In this communication we have investigated the structure of $^{18,20}\text{C}$ using hyperspherical harmonics expansion method assuming $^{16,18}\text{C} + n + n$ three-body model. Standard GPT [30] potential is chosen for the $n - n$ pair while a three-term Gaussian SBB potential [31] with adjustable range parameter is used to compute the ground state energy and wavefunction. The one parameter family of isospectral potentials constructed using the ground state wavefunctions successfully explains the resonance states in both the systems. The method is a robust one and

can be applied for any weakly bound system even if the system lacks any bound ground state.

Acknowledgments

This work has been supported by computational facility at Aliah University, India.

References

- [1] I. Tanihata et al 1985 *Phys. Rev. Lett.* **55** N0.24, 2676
- [2] N. Kobayashi *et al* 2012 *Phys. Rev. C.* **86** 054604
- [3] W. S. Hwash 2017 *Turk. J. Phys.* **41** 151-159
- [4] A. S. Jensen and K. Riisager 2000 *Phys. Lett.* **B480**, No. 1, 39-44
- [5] W. Schwab et al 2000 *Z. Phys.* A350 (1995) 283
- [6] K. Tanaka *et al.* 2010 *Phys. Rev. Lett.* **104** 062701
- [7] G. Audi et al 2003 *Nucl. Phys. A* **729**, No.1, 3-128
- [8] B. Acharya, C. Ji, D.R. Phillips 2013 *Phys. Lett. B.* **723** 196
- [9] Gaudefroy, L. et al. Direct mass measurements of ^{19}B , ^{22}C , ^{29}F , ^{31}Ne , ^{34}Na and other light exotic nuclei. *Phys. Rev. Lett.* 109, 202503 (2012).
- [10] Togano, Y. et al. Interaction cross section study of the two-neutron halo nucleus ^{22}C . *Physics Letters B* 761, 412 – 418 (2016).
- [11] Daniel Sääf and Christian Forssen (2014) *Phys. Rev.* **C89**, No.1, 011303(R)
- [12] A. V. Nesterov et al 2010 *Phys. of Part. and Nuclei* **41** No.5, 716-765
- [13] S. Korennov and Pierre Descouvemont 2004 *Nucl. Phys.* A740, No.3, 249-267
- [14] A. Cobis, D. V. Federov and A. S. Jensen 1997 *Phys. Rev. Lett.* **79**, 2411;
A. Cobis, D.V. Federov and A.S. Jensen 1998 *Phys. Rev. C* **58**, 1403
- [15] A. Csótó 1993 *Phys. Lett.* **B315**. 24; 1993 *Phys. Rev.* **C48** 165; A. Csótó 1993 *ibid.* **C48** 165; A. Csótó 1994 *ibid.* **C49** 3035
- [16] S. Aoyama, S. Mukai, K. Kato and K. Ikeda 1995 *Prog. Theor. Phys.* **94** 343
- [17] N. Tanaka, Y. Suzuki, K. Varga 1997 *Phys. Rev.* C56, 562
- [18] V. Vasilevsky, A. V. Nesterov, F. Arickx, J.Broeckhove 2001 *Phys. Rev.* C63, 034607
- [19] Kazuyuki Ogata, Takayuki Myo, Takenori Furumoto, Takuma Matsumoto, and Masanobu Yahiro 2013 *Phys. Rev. C.* **88** 024616
- [20] Danilin, B. V., Rogde, T., Ershov, S. N., Heiberg-Andersen, H., Vaagen, J. S., Thompson, I. J., Zhukov, M. V. 1997 *Phys. Rev.* C55, R577
- [21] M. Fabre de la Ripelle et al 1982 *Ann. Phys.* **138**, 275-318; T. K. Das, H. T. Coelho, and M. Fabre de la Ripelle 1982 *Phys. Rev. C* **26**, 2288
- [22] T. R. Schneider 1972 *Phys. Letts. B* **40**, 439
- [23] J. L. Ballot, M. Fabre de la Ripelle, and J.S. Levinger 1982 *Phys. Rev. C* **26**, 2301
- [24] T. K. Das, H. T. Coelho and M. Fabre de la Ripelle 1982 *Phys. Rev. C* **26**, 2281
- [25] F. Cooper, A. Khare and U. Sukhatame 1995 *Phys. Rep.* **251**, 267
- [26] A. Khare, U. Sukhatme 1989 *J. Phys. A* **22**, 2847
- [27] M. M. Nieto 1984 *Phys. Lett. B* **145**, 208
- [28] G. Darboux 1882 *C. R. Acad. Sci. Paris* **94**, 1456
- [29] T. K. Das and B. Chakrabarti 2001 *Phys. Letts. A* **288**, 4
- [30] D. Gogny, P. Pires and R. de Turreil 1970 *Phys. Letts.* **32B**, 591
- [31] S. Sack, L. C. Biedenharn and G. Breit 1954 *Phys. Rev.* **93**, 321
- [32] T. K. Das, R. Chattopadhyay, and P.K. Mukherjee 1994 *Phys. Rev. A* **50**, 3521
- [33] Md. A. Khan 2012 *Eur. Phys. Jour.D* **66** 83
- [34] Md. A. Khan and T. K. Das 2001 *Pramana- J. Phys.* **57**, 701
- [35] G. Audi et al., 2003, *Nucl. Phys. A* **729**, 337
- [36] T. Yamaguchi, K. Tanaka et al, 2011, *Nucl.Phys. A*, **864**, 1
- [37] A. Ozawa et al., 2001, *Nucl. Phys. A* **691**, 599

6. Tables

Table 1. Two neutron separation energies, their relative convergence and rms matter radius of ^{18}C and ^{20}C for different K_{max} in their ground states.

<i>System</i> K_{max}	^{18}C ($^{16}\text{C}+n+n$)			^{20}C ($^{18}\text{C}+n+n$)		
	S_{2n} (MeV)	Rel. Convergence	R_A	S_{2n} (MeV)	Rel. Convergence	R_A
4	3.97843	0.10341	2.8297	2.55712	0.15771	2.9832
8	4.43727	0.03861	2.7913	3.03591	0.05480	2.9431
12	4.61546	0.02521	2.7647	3.21193	0.03493	2.9145
16	4.73481	0.01344	2.7425	3.32818	0.01944	2.8867
20	4.79933	0.00638	2.7233	3.39416	0.00984	2.8628
24	4.83013		2.7156	3.42789		2.8479

7. Graphs and Figures

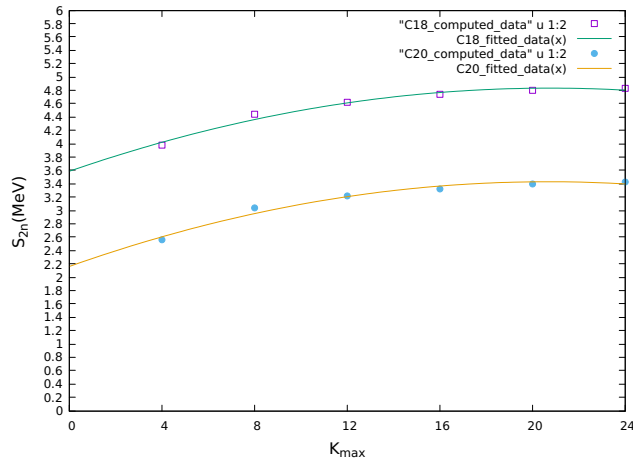


Figure 1. Plot of two-neutron separation energy (S_{2n}) as a function of K_{max} for ^{18}C (upper curve) and ^{20}C (lower curve).

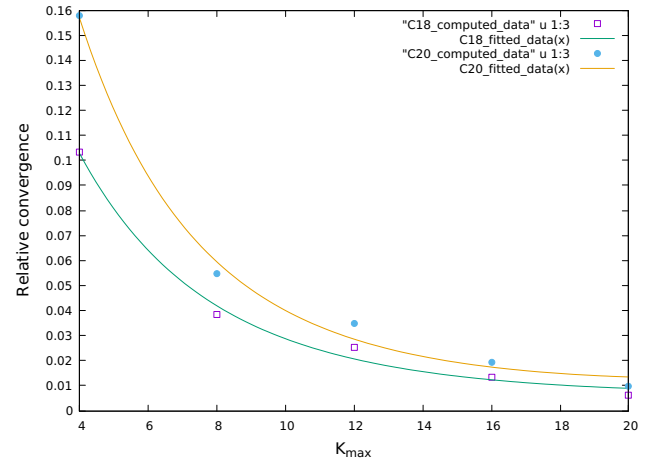


Figure 2. Plot of relative convergence rate with respect to increasing K_{max} for ^{18}C (lower curve) and ^{20}C (upper curve).

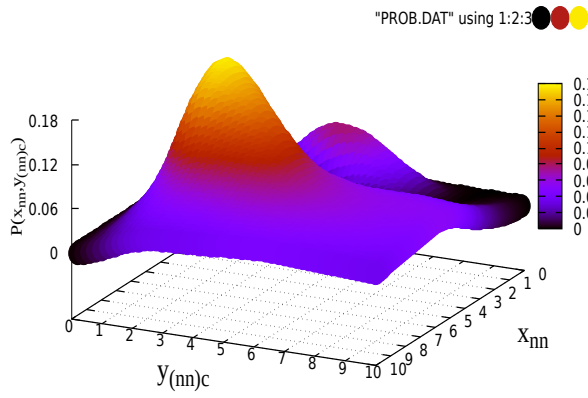


Figure 3. Correlation density plot for the ground state (0^+) state of 2n-halo ^{18}C nucleus as a function of the Jacobi coordinates x_{nn} and $y_{(nn)c}$.

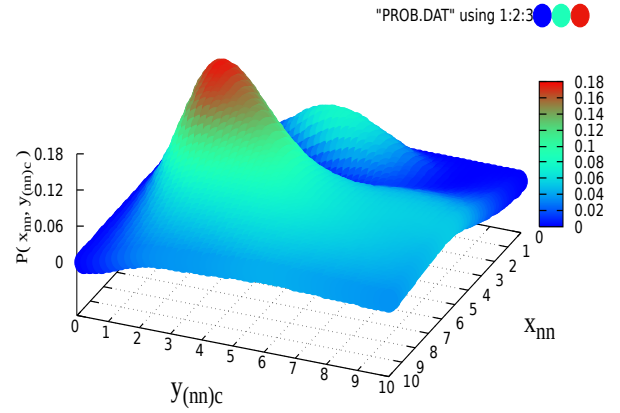


Figure 4. Correlation density plot for the ground state (0^+) state of 2n-halo ^{20}C nucleus as a function of the Jacobi coordinates x_{nn} and $y_{(nn)c}$.

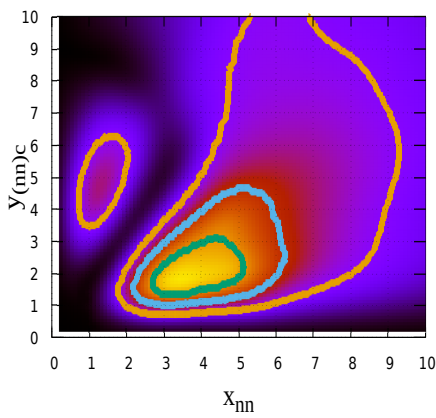


Figure 5. 2D projection of the correlation density plot for the 0^+ state of 2n-halo ^{18}C nucleus as a function of the Jacobi coordinates x_{nn} and $y_{(nn)c}$.

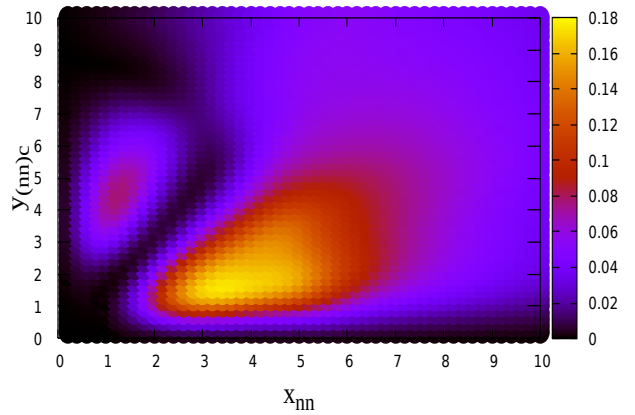


Figure 6. 2D projection of the correlation density plot for the 0^+ state of 2n-halo ^{20}C nucleus as a function of the Jacobi coordinates x_{nn} and $y_{(nn)c}$.

Table 2. Extrapolated values of two-neutron separation energies and their relative convergences for the ground ($J^\pi=0^+$) state of ^{18}C and ^{20}C .

<i>System</i>	^{18}C ($^{16}\text{C}+\text{n}+\text{n}$)		^{20}C ($^{18}\text{C}+\text{n}+\text{n}$)	
	$S_{2n}(\text{MeV})$	Rel. Convergence	$S_{2n}(\text{MeV})$	Rel. Convergence
24	4.83013120	0.00456309	3.42789570	0.00669549
28	4.85227259	0.00303493	3.45100186	0.00446219
32	4.86704371	0.00209706	3.46646992	0.00308899
36	4.87727164	0.00149547	3.47721099	0.00220653
40	4.88457636	0.00109515	3.48490054	0.00161829
44	4.88993151	0.00082034	3.49054929	0.00121388
48	4.89394622	0.00062664	3.49479156	0.00092838
52	4.89701487	0.00048691	3.49803908	0.00072217
56	4.89940043	0.00038406	3.50056708	0.00057019
60	4.90128282	0.00030700	3.50256423	0.00045621
64	4.90278798	0.00024834	3.50416285	0.00036934
68	4.90400585	0.00020305	3.50545757	0.00030221
72	4.90500182	0.00016763	3.50651729	0.00024967
76	4.90582420	0.00013961	3.50739299	0.00020807
80	4.90650922	0.00011721	3.50812293	0.00017479
84	4.90708439	0.00009913	3.50873623	0.00014791
88	4.90757089	0.00008441	3.50925527	0.00012599
92	4.90798515	0.00007231	3.50969749	0.00010800
96	4.90834009	0.00006232	3.51007659	0.00009311
100	4.90864598	0.00005399	3.51040343	0.00008069
104	4.90891099	0.00004693	3.51068673	0.00007028
108	4.90914137	0.00004119	3.51093349	0.00006149
112	4.90934358	0.00003612	3.51114943	0.00005405
116	4.90952089	0.00003186	3.51133920	0.00004769
120	4.90967732	0.00002821	3.51150666	0.00004224
124	4.90981582	0.00002507	3.51165499	0.00003755
128	4.90993891	0.00002235	3.51178684	0.00003349
132	4.91004866	0.00001999	3.51190444	0.00002996
136	4.91014683	0.00001794	3.51200967	0.00002689
140	4.91023492	0.00001614	3.51210410	0.00002419
144	4.91031418	0.00001456	3.51218909	0.00002184
148	4.91038569	0.00001318	3.51226579	0.00001976
152	4.91045039	0.00001195	3.51233519	0.00001792
156	4.91050905	0.00001086	3.51239814	0.00001629
160	4.91056237	0.00000989	3.51245537	0.00001484
164	4.91061094	0.00000903	3.51250750	0.00001355
168	4.91065528	0.00000826	3.51255511	0.00001239
172	4.91069584	0.00000757	3.51259866	0.00001137
176	4.91073301	0.00000695	3.51263858	0.00001044
180	4.91076715	0.00000639	3.51267525	0.00000960
184	4.91079855	0.00000589	3.51270898	0.00000885
188	4.91082748	0.00000544	3.51274007	0.00000817
192	4.91085418	0.00000503	3.51276876	0.00000755
196	4.91087887	0.00000465	3.51279529	0.00000699
200	4.91090172		3.51281985	
.....
∞	4.91124921		3.51319416	

Table 3. Partial contribution of different l_x partial waves to the two-neutron separation energy in the ground states of ^{18}C and ^{20}C corresponding to different K_{max} .

<i>System</i>	^{18}C					^{20}C				
	E_{l_x} for $l_x=$					E_{l_x} for $l_x=$				
	0	1	2	3	4	0	1	2	3	4
4	2.886	0.068	1.149	0.000	0.000	2.471	0.235	0.036	0.000	0.000
8	3.283	0.072	1.158	0.001	0.100	2.902	0.232	0.019	1.034	0.001
12	3.414	0.078	1.158	0.001	0.098	3.073	0.231	0.014	1.036	0.001
16	3.487	0.079	1.166	0.001	0.098	3.1948	0.2278	0.0136	1.040	0.001
20	3.536	0.081	1.181	0.001	0.096	3.262	0.225	0.013	1.049	0.001
24	3.566	0.082	1.199	0.001	0.094	3.295	0.225	0.013	1.080	0.001

Table 4. Data to show the effects of the parameter λ on the depth of the well and height of the barrier, in the isospectral potential constructed from the lowest eigen potential and the corresponding wavefunction for ^{18}C and ^{20}C .

<i>System</i>	^{18}C				^{20}C			
	Potential Well		Potential Barrier		Potential Well		Potential Barrier	
	<i>Depth, V_0</i> (<i>MeV</i>)	<i>At, r</i> (<i>fm</i>)	<i>Height, V_B</i> (<i>MeV</i>)	<i>At, r</i> (<i>fm</i>)	<i>Depth, V_0</i> (<i>MeV</i>)	<i>At, r</i> (<i>fm</i>)	<i>Height, V_B</i> (<i>MeV</i>)	<i>At, r</i> (<i>fm</i>)
100000	-9.301	3.092	2.702	20.099	-11.076	3.069	3.085	7.520
100	-9.311	3.092	2.712	20.099	-11.086	3.069	3.094	7.514
50	-9.337	3.091	2.712	20.099	-11.163	3.065	3.106	7.504
1	-11.590	3.019	2.719	20.095	-17.294	2.824	3.938	6.708
0.1	-24.220	2.664	5.394	5.088	-41.931	2.320	10.924	3.983
0.01	-62.846	2.109	19.797	3.424	-95.444	1.811	36.751	2.840
0.001	-136.144	1.637	56.596	2.521	-154.453	1.389	84.198	2.173
0.0001	-247.602	1.274	121.482	1.937	-270.962	1.000	141.518	1.731
0.00001	-384.056	0.986	218.025	1.520	-479.005	0.724	241.024	1.218

Table 5. Comparison of the calculated data with those found in the literature for ^{18}C and ^{20}C halo nuclei.

Nuclide	State	Observables	Present work	Others work
^{18}C	0^+	BE	4.9064 MeV	4.910 ± 0.030 MeV[35] 4.91 MeV[36]
		R_A	2.7156 fm	2.82 ± 0.04 fm[37]
	0_1^+	E_R	1.89 MeV	-
^{20}C	0^+	BE	3.5065 MeV	3.510 ± 0.240 MeV[35] 3.51 MeV[36]
		R_A	2.8479 fm	2.98 ± 0.05 fm [37]
	0_1^+	E_R	3.735 MeV	-

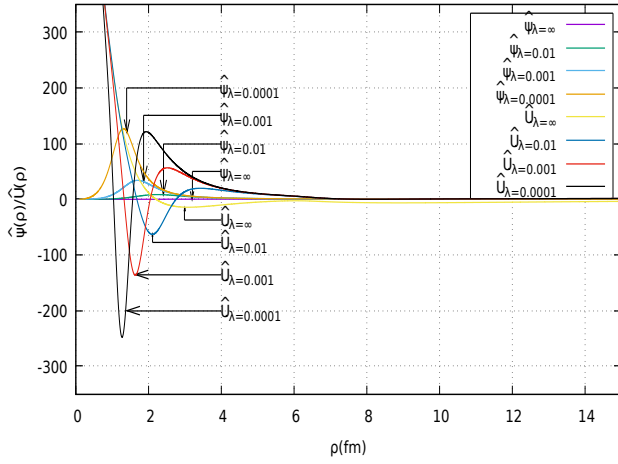


Figure 7. Graphical presentation of potentials and corresponding wavefunctions of ^{18}C for few representative values of λ ($= \infty$ (original potential), 0.01, 0.001 and 0.0001).

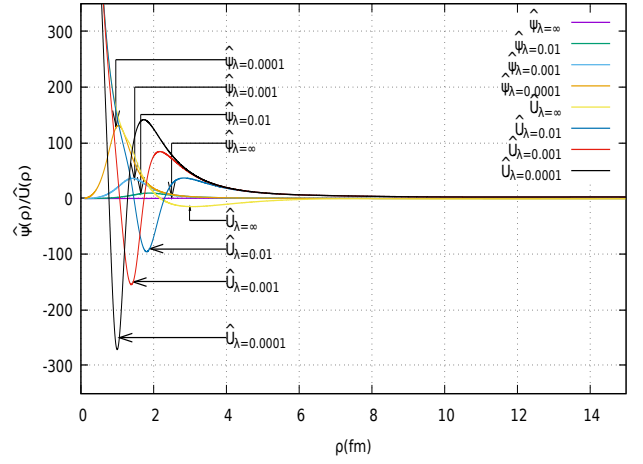


Figure 8. Graphical presentation of potentials and corresponding wavefunctions of ^{20}C for few representative values of λ ($= \infty$ (original potential), 0.01, 0.001 and 0.0001).

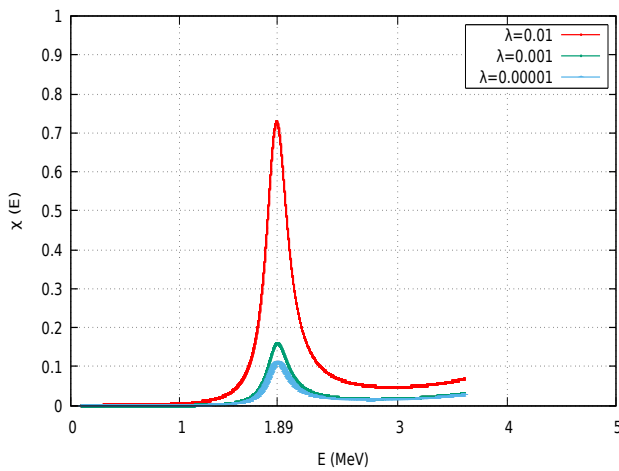


Figure 9. Plot of $G(E)$ as a function of energy demonstrating the resonant state(s) in ^{18}C .

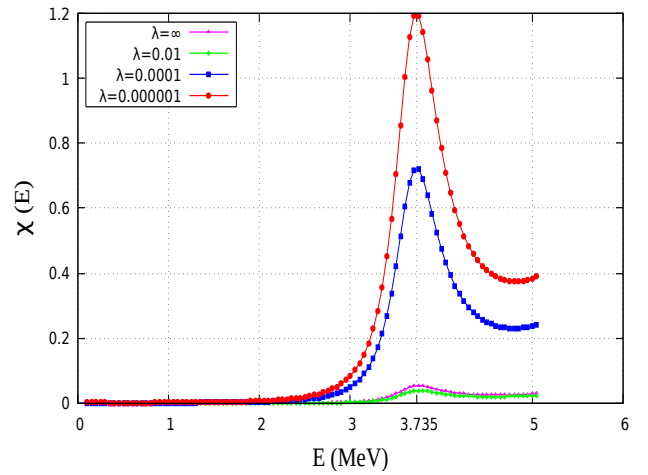


Figure 10. lot of $G(E)$ as a function of energy demonstrating the resonant state(s) in ^{20}C .